Stabilization of the Trigonal High-Temperature Phase of Formamidinium Lead Iodide

ARTICLE *in* JOURNAL OF PHYSICAL CHEMISTRY LETTERS · APRIL 2015

Impact Factor: 7.46 · DOI: 10.1021/acs.jpclett.5b00380

THE JOURNAL OF PHYSICAL CHEMISTRY Letters

Letter

pubs.acs.org/JPCL

Stabilization of the Trigonal High-Temperature Phase of Formamidinium Lead Iodide

Andreas Binek, Fabian C. Hanusch, Pablo Docampo, and Thomas Bein*

Department of Chemistry and Center for NanoScience (CeNS), University of Munich (LMU) Butenandtstr. 5−13 (Haus E), 81377 Munich, Germany

Supporting Information

ABSTRACT: Formamidinium lead iodide ($FAPbI_3$) has the potential to achieve higher performance than established perovskite solar cells like methylammonium lead iodide ($MAPbI_3$), while maintaining a higher stability. The major drawback for the latter material is that it can crystallize at room temperature in a wide bandgap hexagonal symmetry ($P6_3mc$) instead of the desired trigonal ($P3m1$) black phase formed at a higher temperature (130 °C). Our results show that employing a mixture of MAI and FAI in films deposited via a two-step approach, where the MAI content is <20%, results in the exchange of FA molecules with MA without any significant lattice shrinkage. Additionally, we show with temperature-dependent X-ray diffraction that the trigonal phase exhibits no phase changes in the temperature range studied (25 to 250 °C). We attribute the stabilization of the structure to stronger interactions between the MA cation and the inorganic cage. Finally, we show that the inclusion of this small amount of MA also has a positive effect on the lifetime of the photoexcited species and results in more efficient devices.

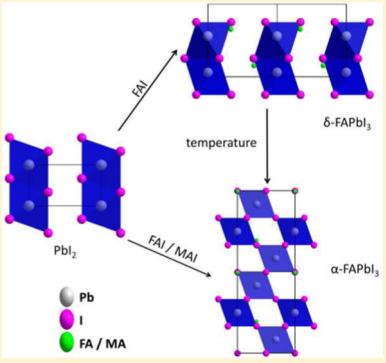

With the recent rise in awareness of environmental and energy issues, the development of renewable energy sources has been the focus of a large number of research groups. Over the last 2 years, solar cells based on alkylammonium lead halide perovskites have distinguished themselves as a highly efficient and inexpensive photovoltaic technology.[1−4] Because these materials are solution-processable in a facile way at low temperatures, solar cells on flexible substrates can be prepared with high photovoltaic performance.[5−8] Current state-of-the-art devices are based on the methylammonium lead iodide ($MAPbI_3$) perovskite, with a certified power conversion efficiency (PCE) of 19.3%.[9]

However, the long-term stability of the prepared devices is an open question because $MAPbI_3$ undergoes a reversible phase transition between tetragonal and cubic symmetry in a temperature range between 54 and 57 °C, corresponding to common solar cell operating temperatures during summer.[10] This structural phase transition is expected to influence the electronic band structure of the material and therefore impact the photovoltaic properties.[10] The development of a perovskite without temperature-induced phase transitions in this temperature range is required to achieve a stable solar cell in the long term.

The exchange of the organic cation of the perovskite from methylammonium (MA) to formamidinium (FA) results in a material with either a trigonal structure (black color, α phase) or a hexagonal structure (yellow color, δ phase) depending on the synthesis temperature. For the δ phase, no significant phase transition is expected within the solar cell operating temperature range because the phase transition from the δ phase to the α phase takes place at ∼125 °C.[11] Furthermore, the larger cation influences the metal−halide−metal bond angle, which leads to a narrower bandgap relative to $MAPbI_3$.[12] Therefore, $FAPbI_3$ is closer to the optimum bandgap for a single junction solar cell derived from the Shockley−Queisser limit, which in turn leads to potentially higher theoretical efficiencies.[13] Pellet and coworkers used this concept to extend the optical-absorption onset of $MAPbI_3$ into the red region by incorporating FA into the structure.[14] Jeon et al. have recently adapted this strategy by mixing $FAPbI_3$ with $MAPbBr_3$, achieving PCEs of 18%.[15] However, in this instance, one of the advantages of using $FAPbI_3$, that is, its narrower bandgap, is lost by the combination with a bromide compound.[16,17] Moreover, the introduction of bromide will per se change the lattice constant of the perovskite, thus making it more challenging to isolate the impact of the inclusion of methylammonium in the structure. Additionally, the devices developed in Jeon et al.'s study incorporate a mesoporous titania photoanode, which could preclude its inclusion in tandem or flexible applications. Concluding from Pellet's and Jeon's studies, a transition from tetragonal (i.e., similar to $MAPbI_3$) to trigonal symmetry (i.e., similar to α-$FAPbI_3$) is observed when the methylammonium content in the structure is reduced to <20%.[14,15]

Here we explore this route to stabilize the α phase of $FAPbI_3$ for its application in planar heterojunction solar cells without the need for high annealing temperatures. We show that

Received: February 21, 2015
Accepted: March 16, 2015
Published: March 16, 2015

DOI: 10.1021/acs.jpclett.5b00380
J. Phys. Chem. Lett. 2015, 6, 1249−1253

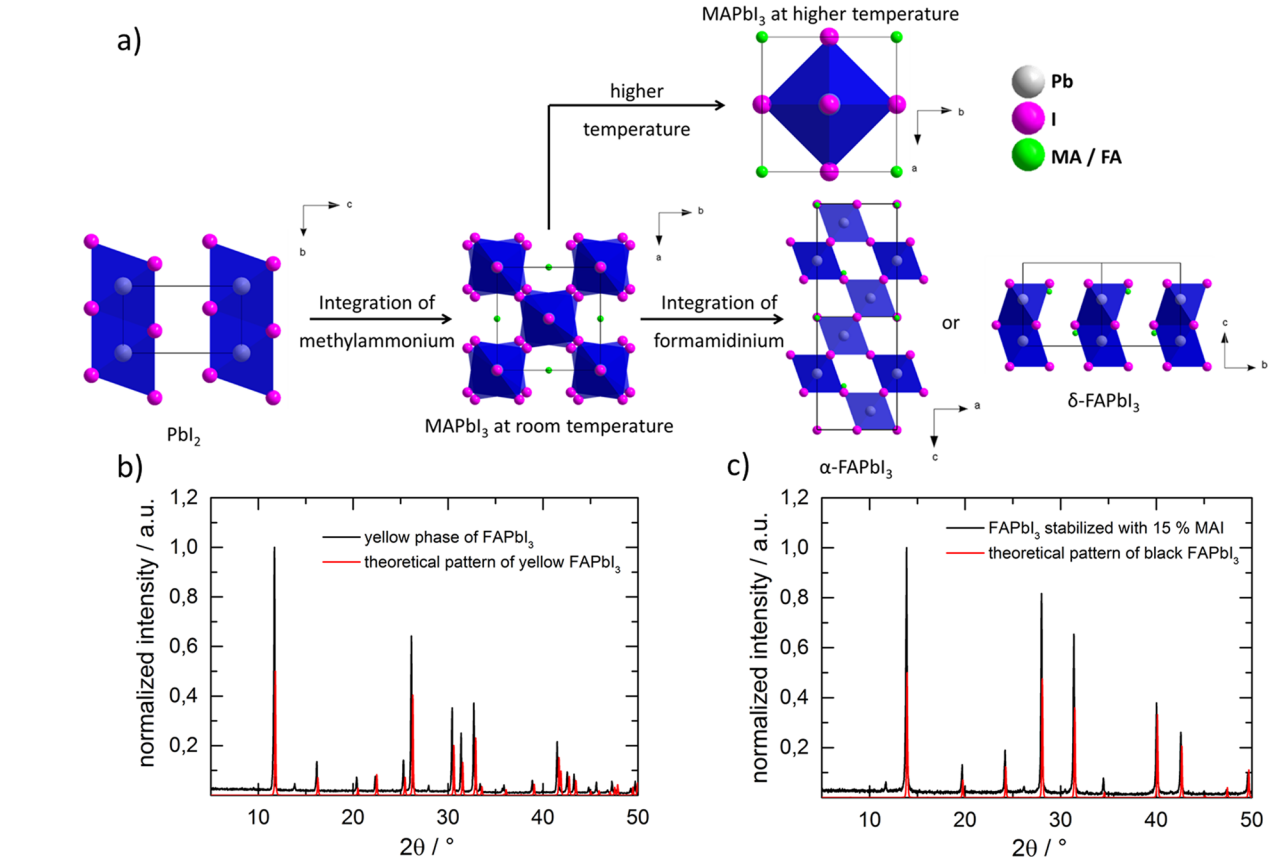

Figure 1. Crystal structure of PbI_2 and $MAPbI_3$ at different temperatures, α-$FAPbI_3$ and δ-$FAPbI_3$ (a) and the corresponding wide angle XRD pattern of the yellow δ-phase (b) and the stabilized black α-phase (c) of $FAPbI_3$. The intensity of the theoretical patterns was reduced by half to illustrate the comparison of the XRD patterns.

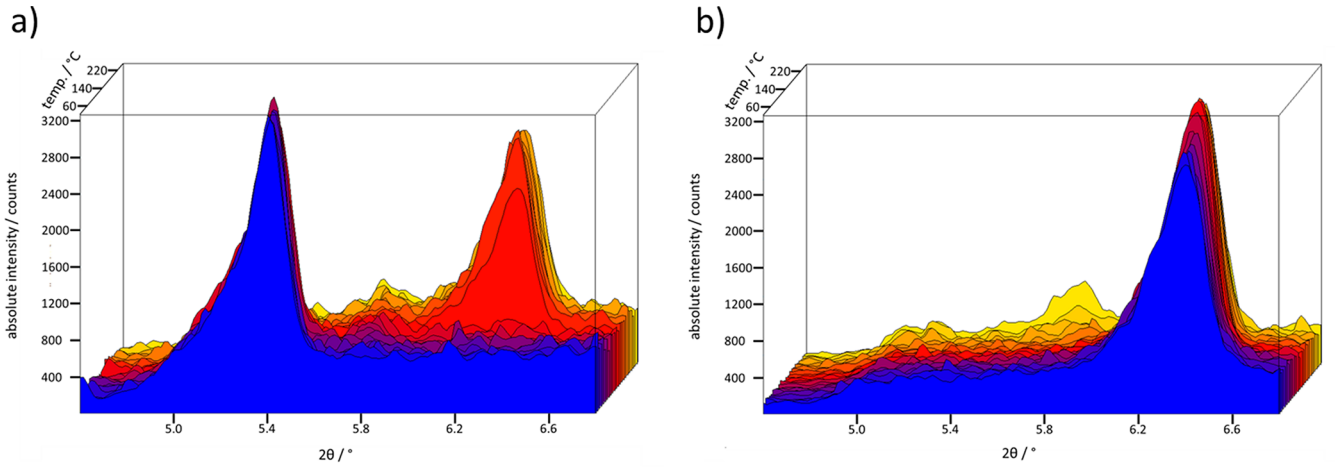

Figure 2. Temperature-dependent X-ray diffraction measurements of non-stabilized $FAPbI_3$ with phase transition (a) and stabilized $FAPbI_3$ (b) without phase transition.

incorporation of a smaller cation (MA) with a high dipole moment stabilizes the trigonal phase of $FAPbI_3$ without any lattice shrinkage or changes in the optical properties. We ascribe this finding to the enhancement of I−H hydrogen bonds between the cation and the inorganic cage or to an increase in the Madelung energy of the structure. Thereby, the δ phase transition can be completely suppressed, as shown by temperature-dependent X-ray diffraction. Our results help to elucidate the origin of the improved performance and the stability of the newly developed systems.

The stabilized $FAPbI_3$ samples were prepared via a two-step deposition/conversion process. A layer of lead iodide (PbI_2) was initially deposited on an FTO-covered glass substrate via spin-coating and subsequently converted into the perovskite phase in a second step by immersion in a solution of 85% FAI and 15% MAI in isopropanol (IPA). The crystal structures of the starting material, PbI_2, as well as of $MAPbI_3$ and $FAPbI_3$ are shown in Figure 1a to illustrate the differences between $MAPbI_3$ and $FAPbI_3$. For PbI_2, the PbI_6 octahedra are connected via a shared plane of three iodide ions. Through

DOI: 10.1021/acs.jpclett.5b00380
J. Phys. Chem. Lett. 2015, 6, 1249−1253

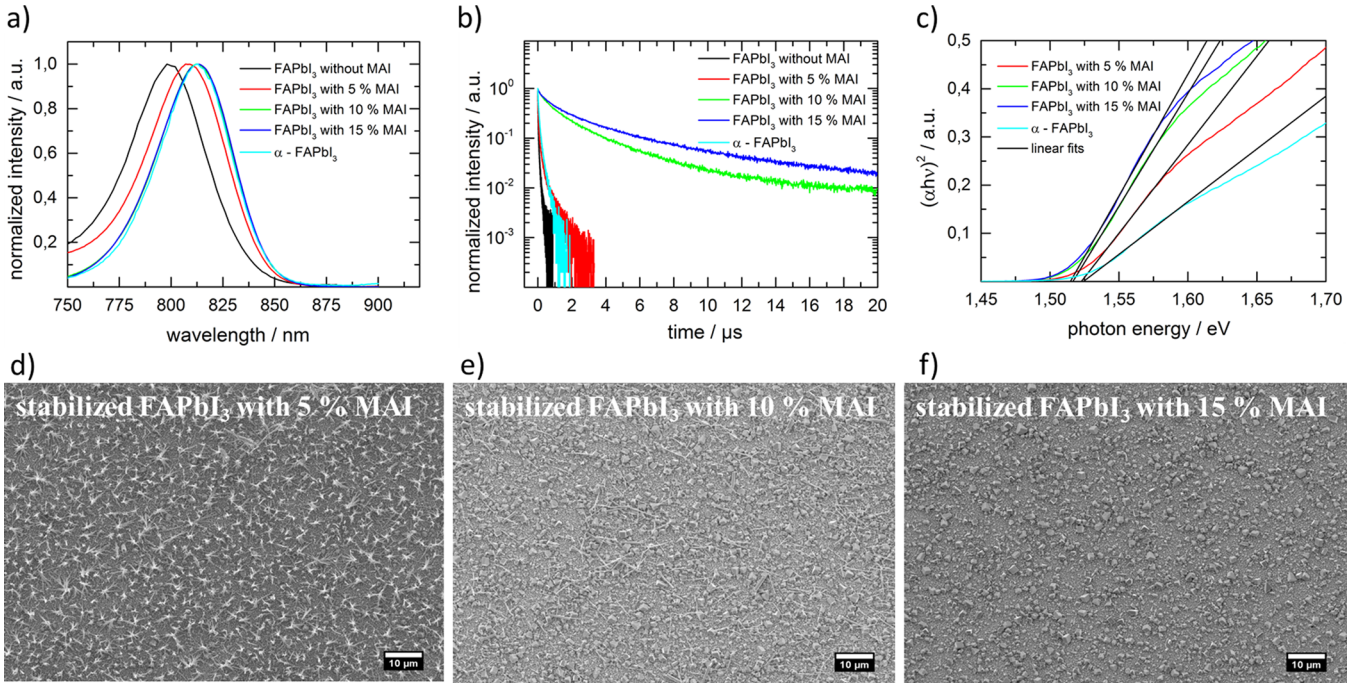

Figure 3. Photoluminescence measurements (a), time-correlated single-photon counting measurements (b), and Tauc plots (c) of samples with different concentrations of MAI. The estimated bandgap for all MAI concentrations and α-$FAPbI_3$ is 1.52 ± 0.02 eV. SEM micrographs of stabilized $FAPbI_3$ with 5% MAI (d), 10% MAI (e), and 15% MAI (f). With increasing MA content the needle-like structure disappears and is replaced by a cubic structure.

the incorporation of MA, the layered octahedra form a 3D network by reducing the number of shared iodide ions from three to only one; however, at room temperature the octahedra are not perfectly aligned, which results in an identical twist of every second octahedral layer in the *c* direction. When the temperature increases, the unit cell expands and the octahedra will arrange perfectly along the *c* axis. This effect can also be observed when filling the unit cell with a mixture of MA and FA. While still maintaining the tetragonal room temperature structure, the unit cell is enlarged. This was observed in X-ray diffraction measurements by a shift of the diffraction pattern to lower angles.[14] With >80% of FA in the perovskite structure, the tetragonal symmetry collapses and the trigonal structure of α-$FAPbI_3$ is formed. In this configuration the octahedra form a 3D network. However, at room temperature the neat $FAPbI_3$ compound can also crystallize in a hexagonal structure (δ-$FAPbI_3$), where the octahedra form a network similar to PbI_2. In Figure 1b,c the XRD patterns of the synthesized yellow $FAPbI_3$ and stabilized black $FAPbI_3$ and their theoretical patterns are illustrated.[11]

The comparison of theoretical and experimental XRD patterns for the prepared samples shows that both $FAPbI_3$ structures were successfully prepared. Temperature-dependent X-ray diffraction measurements were performed on both a non-stabilized and a stabilized sample to monitor the stabilization of the α phase of $FAPbI_3$. The phase transition can be observed in the shift of the main reflection to higher angles (from 5.4° 2θ to 6.3° 2θ) because the unit cell of the α phase is larger than the unit cell of the δ phase. Temperature-dependent XRD measurements with powder samples (Figure 2) were performed with a molybdenum source. The diffraction pattern is therefore shifted to lower angles compared with the XRD patterns in Figure 1, which were obtained using Cu–$K_{\alpha 1}$ radiation. The main reflection for the δ-phase is at 5.4° 2θ, and for the α-phase this reflection is at 6.3° 2θ.

In the non-stabilized sample, the phase transition occurs at 130 °C, which is slightly higher than the observed temperature for single crystals of $FAPbI_3$ (125 °C).[11] The phase transition was reversible, where upon cooling to room temperature the sample returned to the original δ phase. The measurement of the MA-stabilized sample of $FAPbI_3$ was performed in the same temperature range. In contrast with the neat $FAPbI_3$ sample, no phase transition from the trigonal α-$FAPbI_3$ was observed in this temperature range. We note here that previous studies demonstrate phase-pure α-$FAPbI_3$ at room temperature;[10] however, these films were prepared on mesoporous TiO_2. The use of a mesoporous scaffold may influence the crystal structure of the perovskite and possibly alter its phase transition due to the confinement in TiO_2 mesopores.[18] The sample preparation and the temperature-dependent XRD measurements were performed under a nitrogen atmosphere, and thus the influence of water can be excluded as a cause for the formation of δ-$FAPbI_3$. At concentrations of MA below 15% in the conversion solution, both α-$FAPbI_3$ and δ-$FAPbI_3$ were formed; see Supporting Information (SI) Figure S1. The disappearance of the yellow δ-$FAPbI_3$ phase can also be monitored via the SEM micrographs in Figure 3d–f. Here the needle-like crystals formed at lower MA content can be assigned to the δ-$FAPbI_3$ phase, as they correlate with the disappearance of the XRD reflections corresponding to the hexagonal structure when α-$FAPbI_3$ is stabilized with higher amounts of MA.

The photophysical properties of the materials were measured to further understand the origin of the higher photovoltaic performance of the MA-stabilized compounds. The photoluminescence (PL) spectra of the stabilized samples are illustrated in Figure 3a. In the non-stabilized samples, a PL

DOI: 10.1021/acs.jpclett.5b00380
J. Phys. Chem. Lett. 2015, 6, 1249–1253

emission maximum at 798 nm can be observed. With increasing MAI content, the emission is shifted and matches the position of neat α-$FAPbI_3$ at 813 nm with 10% MAI and 15% MAI in the conversion solution. For the neat δ phase the PL signal was below the detection limit of the instrument and is therefore not shown. Additionally, time-correlated single-photon counting (TCSPC) measurements were performed to obtain the lifetime of the photoexcited species in the prepared films. Figure 3b shows the drastic increase in lifetime for samples with 10 and 15% MAI compared with the non-stabilized $FAPbI_3$, the neat α-$FAPbI_3$, and the 5% MAI sample. This striking difference in lifetime can be attributed to the stabilization of the crystal structure of α-$FAPbI_3$ and the disappearance of the δ phase. We note here that the decay dynamics found for the neat α-$FAPbI_3$ compound are very similar to those found for the standard $MAPbI_3$ compound.[19] As previously mentioned, both structures of $FAPbI_3$ were observed in the XRD measurements for samples with lower MA concentration, with a large number of grain boundaries between both phases. In these crossover samples, traps for the photoexcited species may be located at the grain boundaries and recombination can occur.[20] The lifetime of the photoexcited species can be enhanced by reducing the number of grain boundaries in the perovskite layer. Similar behavior was also reported for a passivation of surface trap states in $MAPbI_3$.[21]

The corresponding UV−vis measurements are shown in Figure S2 in the SI. By fitting the linear part of the plots, a bandgap of 1.52 ± 0.02 eV was estimated for all films (Figure 3c). The bandgap energy found for the films presented here is in good agreement with the value of 1.48 eV estimated by Eperon and coworkers.[16] Because the bandgap of the prepared films was found to be the same for all MAI contents, there is a possibility that no MA was introduced in the crystal structure. To probe this, we performed elemental analysis of the stabilized sample. Neat $FAPbI_3$ should have a nitrogen content of 4.5% and a carbon content of 1.9% of the total compound mass; however, in the stabilized $FAPbI_3$ prepared by substitution with 15% MAI relative to FAI in the conversion solution, the nitrogen content is lower (4.2%) and the carbon content is higher (2.1%), which corresponds to a composition of $FA_{0.87}MA_{0.13}PbI_3$.

The stabilization of the α phase of $FAPbI_3$ can also be monitored in the performance of the solar cells with different MAI concentrations. With increasing MAI content, the short-circuit current (J_{SC}), the open-circuit voltage (V_{OC}), and the fill factor (FF) are enhanced (Figure S3 in the SI). The most efficient device contains 15% MAI and exhibits a high short-circuit current of 15.7 mA and a fill factor of 56% with a voltage of 1 V, resulting in PCE (η) of 8.7%. We note here that the maximum performance of the devices prepared in this work is limited by the rough perovskite layer. The SEM micrographs shown in Figure 3d−f show a full surface coverage for all prepared samples, while all samples exhibit similar absorbance (Figure S2 in the SI). We can therefore exclude shunting between the electron- and hole-selective contacts or thickness variations as the causes for the differences in short-circuit current for the prepared devices. However, the needle-like crystals laying on top of the perovskite layer suggest the formation of the hexagonal structure of $FAPbI_3$ at this interface. This wide-bandgap material may then reduce charge transfer from α-$FAPbI_3$ into the hole transporter and consequently diminish the charge collection efficiency, thus accounting for the observed short-circuit photocurrent differences.

To understand the stabilization of the α-phase of $FAPbI_3$, we consider two possibilities. First, the structure can be made more stable by increasing the number of hydrogen bonds between the iodide ions and the hydrogen of the ammonium moiety in the cation. The probability of hydrogen-bond formation may be related to the number of hydrogen atoms of the molecule, and with four FA ions present in the pseudocubic α-$FAPbI_3$ unit cell,[22] bearing four hydrogen atoms each, this is already quite likely; however, molecules with a higher dipole moment tend to form stronger hydrogen bonds.[22,23] Because MA exhibits a dipole moment ten times higher than FA, 2.3 D compared with 0.21 D,[24] with three hydrogen atoms, we suggest that it is more likely that stronger hydrogen bonds are formed when MA is introduced into the α-$FAPbI_3$ structure. The low dipole moment in FA is due to the resonance stabilization of the structure.[24] In this case, the electron density is homogeneously distributed over the nitrogen−carbon−nitrogen bond, as reported by Frost et al.[24] In contrast, the electron density of the MA molecule is concentrated at the nitrogen atom. Second, the structure can be made more stable through the increase in the Madelung energy.[25] Because the Coulombic interaction between charges and dipoles is proportional to the strength of the dipole, in this second scenario it is possible that the stronger interaction between MA and the lead iodide octahedra results in an increase in the Madelung energy and therefore to an enhanced stability of the system.[26] Both cations and their interactions with the inorganic "cage" are shown in Figure 4.

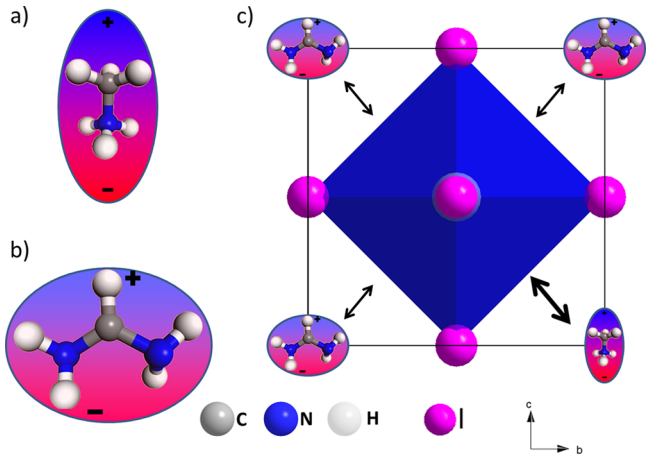

Figure 4. Illustration of the dipole moments of MA (a) and FA (b) and their different influence on the inorganic cage of the perovskite (c).

In summary, we have studied the phase transition of the yellow δ phase to the dark α phase of $FAPbI_3$ in perovskite films prepared by a two-step deposition/conversion method. By exchanging a small amount of 15% MA relative to FA in the immersion solution, we show that the resulting films exhibit a fully stabilized α phase in the temperature range studied (25−250 °C). Elemental analysis of the prepared samples shows a composition of $FA_{0.87}MA_{0.13}PbI_3$. Strikingly, no accompanying lattice shrinkage was observed, while the transition to the yellow δ phase of $FAPbI_3$ was completely suppressed in the temperature range examined. We suggest that the smaller MA cation, which exhibits a dipole moment 10 times larger than FA, stabilizes the 3D arrangement of the PbI_6 octahedra with a pseudocubic symmetry via I−H hydrogen bonding or the increase in Coulomb interactions within the structure. This also

DOI: 10.1021/acs.jpclett.5b00380
J. Phys. Chem. Lett. 2015, 6, 1249−1253

results in additional benefits for solar-cell performance in the form of a drastic increase in the lifetime of the photoexcited species generated within the film and a corresponding high device performance. The dipole moment of the cation is an important parameter for the formation of hybrid perovskites; therefore, this approach is expected to be suitable for the stabilization of other perovskite systems for further enhancement of the crystallization of the active layer and their application in photovoltaic devices.

■ ASSOCIATED CONTENT

Supporting Information

Further crystalographic analysis, optical characterization, and *J*/*V* measurements. This material is available free of charge via the Internet at http://pubs.acs.org.

■ AUTHOR INFORMATION

Corresponding Author

*E-mail: bein@lmu.de. Fax: +49-89-2180-77622.

Notes

The authors declare no competing financial interest.

■ ACKNOWLEDGMENTS

We thank Thomas Miller from the Chemistry Department of the University of Munich (LMU) for the temperature-dependent X-ray diffraction measurements. We acknowledge funding by the Bavarian State Ministry of the Environment and Consumer Protection, the Bavarian network "Solar Technologies Go Hybrid", and the DFG Excellence Cluster Nanosystems Initiative Munich (NIM). We gratefully acknowledge support from the European Union through the award of a Marie Curie Intra-European Fellowship.

■ REFERENCES

(1) Ball, J. M.; Lee, M. M.; Hey, A.; Snaith, H. J. Low-Temperature Processed Meso-Superstructured to Thin-Film Perovskite Solar Cells. *Energy Environ. Sci.* **2013**, *6*, 1739−1743.

(2) Liu, M.; Johnston, M. B.; Snaith, H. J. Efficient Planar Heterojunction Perovskite Solar Cells by Vapour Deposition. *Nature* **2013**, *501*, 395−398.

(3) Burschka, J.; Pellet, N.; Moon, S.-J.; Humphry-Baker, R.; Gao, P.; Nazeeruddin, M. K.; Gratzel, M. Sequential Deposition As a Route to High-Performance Perovskite-Sensitized Solar Cells. *Nature* **2013**, *499*, 316−319.

(4) Kazim, S.; Nazeeruddin, M. K.; Grätzel, M.; Ahmad, S. Perowskit als Lichtabsorptionsmaterial: ein Durchbruch in der Photovoltaik. *Angew. Chem.* **2014**, *126*, 2854−2867.

(5) Docampo, P.; Ball, J. M.; Darwich, M.; Eperon, G. E.; Snaith, H. J. Efficient Organometal Trihalide Perovskite Planar-Heterojunction Solar Cells on Flexible Polymer Substrates. *Nat. Commun.* **2013**, *4*, 2761.

(6) You, J.; Hong, Z.; Yang, Y.; Chen, Q.; Cai, M.; Song, T.-B.; Chen, C.-C.; Lu, S.; Liu, Y.; Zhou, H.; Yang, Y. Low-Temperature Solution-Processed Perovskite Solar Cells with High Efficiency and Flexibility. *ACS Nano* **2014**, *8*, 1674.

(7) Chiang, Y.-F.; Jeng, J.-Y.; Lee, M.-H.; Peng, S.-R.; Chen, P.; Guo, T.-F.; Wen, T.-C.; Hsu, Y.-J.; Hsu, C.-M. High Voltage and Efficient Bilayer Heterojunction Solar Cells Based on Organic-Inorganic Hybrid Perovskite Absorber with Low-Cost Flexible Substrate. *Phys. Chem. Chem. Phys.* **2014**, *16*, 6033.

(8) Lee, M. M.; Teuscher, J.; Miyasaka, T.; Murakami, T. N.; Snaith, H. J. Efficient Hybrid Solar Cells Based on Meso-Superstructured Organometal Halide Perovskites. *Science* **2012**, *338*, 643−647.

(9) Zhou, H.; Chen, Q.; Li, G.; Luo, S.; Song, T.-b.; Duan, H.-S.; Hong, Z.; You, J.; Liu, Y.; Yang, Y. Interface Engineering of Highly Efficient Perovskite Solar Cells. *Science* **2014**, *345*, 542−546.

(10) Baikie, T.; Fang, Y. N.; Kadro, J. M.; Schreyer, M.; Wei, F. X.; Mhaisalkar, S. G.; Graetzel, M.; White, T. J. Synthesis and Crystal Chemistry of the Hybrid Perovskite (CH3NH3) PbI3 for Solid-State Sensitised Solar Cell Applications. *J. Mater. Chem. A* **2013**, *1*, 5628−5641.

(11) Stoumpos, C. C.; Malliakas, C. D.; Kanatzidis, M. G. Semiconducting Tin and Lead Iodide Perovskites with Organic Cations: Phase Transitions, High Mobilities, and Near-Infrared Photoluminescent Properties. *Inorg. Chem.* **2013**, *52*, 9019−9038.

(12) Filip, M. R.; Eperon, G. E.; Snaith, H. J.; Giustino, F. Steric Engineering of Metal-Halide Perovskites with Tunable Optical Band Gaps. *Nat. Commun.* **2014**, *5*, 5757.

(13) Shockley, W.; Queisser, H. J. Detailed Balance Limit of Efficiency of p-n Junction Solar Cells. *J. Appl. Phys.* **1961**, *32*, 510−519.

(14) Pellet, N.; Gao, P.; Gregori, G.; Yang, T.-Y.; Nazeeruddin, M. K.; Maier, J.; Grätzel, M. Mixed-Organic-Cation Perovskite Photovoltaics for Enhanced Solar-Light Harvesting. *Angew. Chem., Int. Ed.* **2014**, *53*, 3151−3157.

(15) Jeon, N. J.; Noh, J. H.; Yang, W. S.; Kim, Y. C.; Ryu, S.; Seo, J.; Seok, S. I. Compositional Engineering of Perovskite Materials for High-Performance Solar Cells. *Nature* **2015**, *517*, 476−480.

(16) Eperon, G. E.; Stranks, S. D.; Menelaou, C.; Johnston, M. B.; Herz, L.; Snaith, H. Formamidinium Lead Trihalide: A Broadly Tunable Perovskite for Efficient Planar Heterojunction Solar Cells. *Energy Environ. Sci.* **2014**, *7*, 982−988.

(17) Noh, J. H.; Im, S. H.; Heo, J. H.; Mandal, T. N.; Seok, S. I. Chemical Management for Colorful, Efficient, and Stable Inorganic−Organic Hybrid Nanostructured Solar Cells. *Nano Lett.* **2013**, *13*, 1764−1769.

(18) Choi, J. J.; Yang, X.; Norman, Z. M.; Billinge, S. J. L.; Owen, J. S. Structure of Methylammonium Lead Iodide Within Mesoporous Titanium Dioxide: Active Material in High-Performance Perovskite Solar Cells. *Nano Lett.* **2014**, *14*, 127−133.

(19) Docampo, P.; Hanusch, F. C.; Stranks, S. D.; Döblinger, M.; Feckl, J. M.; Ehrensperger, M.; Minar, N. K.; Johnston, M. B.; Snaith, H. J.; Bein, T. Solution Deposition-Conversion for Planar Heterojunction Mixed Halide Perovskite Solar Cells. *Adv. Energy Mater.* **2014**, *4*.

(20) Wu, X.; Trinh, M. T.; Niesner, D.; Zhu, H.; Norman, Z.; Owen, J. S.; Yaffe, O.; Kudisch, B. J.; Zhu, X. Trap States in Lead Iodide Perovskites. *J. Am. Chem. Soc.* **2015**, *137*, 2089−96.

(21) Noel, N. K.; Abate, A.; Stranks, S. D.; Parrott, E.; Burlakov, V.; Goriely, A.; Snaith, H. J. Enhanced Photoluminescence and Solar Cell Performance via Lewis Base Passivation of Organic-Inorganic Lead Halide Perovskites. *ACS Nano* **2014**, *8*, 9815−21.

(22) Amat, A.; Mosconi, E.; Ronca, E.; Quarti, C.; Umari, P.; Nazeeruddin, M. K.; Grätzel, M.; De Angelis, F. Cation-Induced Band-Gap Tuning in Organohalide Perovskites: Interplay of Spin−Orbit Coupling and Octahedra Tilting. *Nano Lett.* **2014**, *14*, 3608−16.

(23) Li, W.; Thirumurugan, A.; Barton, P. T.; Lin, Z.; Henke, S.; Yeung, H. H. M.; Wharmby, M. T.; Bithell, E. G.; Howard, C. J.; Cheetham, A. K. Mechanical Tunability via Hydrogen Bonding in Metal−Organic Frameworks with the Perovskite Architecture. *J. Am. Chem. Soc.* **2014**, *136*, 7801−7804.

(24) Frost, J. M.; Butler, K. T.; Brivio, F.; Hendon, C. H.; van Schilfgaarde, M.; Walsh, A. Atomistic Origins of High-Performance in Hybrid Halide Perovskite Solar Cells. *Nano Lett.* **2014**, *14*, 2584−90.

(25) Madelung, E. Das elektrische Feld in Systemen von regelmäßig angeordneten Punktladungen. *Phys. Z.* **1919**, *19*, 524−533.

(26) Harrison, W. A. *Electronic Structure and the Properties of Solids*; Freeman: San Francisco, 1980

DOI: 10.1021/acs.jpclett.5b00380
J. Phys. Chem. Lett. 2015, 6, 1249−1253